Nanoscale

PAPER

View Article Online
View Journal | View Issue

Cite this: *Nanoscale*, 2019, **11**, 16592

One body, two hands: photocatalytic function- and Fenton effect-integrated light-driven micromotors for pollutant degradation†

Jiajia Wang,‡[a] Renfeng Dong, *‡[a] Qianxian Yang,[a] Huiying Wu,[a] Zijun Bi,[a] Qiying Liang,[a] Qinglong Wang,[a] Chun Wang,[a] Yongfeng Mei *[b] and Yuepeng Cai*[a]

Received 20th May 2019,
Accepted 10th August 2019

DOI: 10.1039/c9nr04295d

rsc.li/nanoscale

The threat of water pollution represents a serious global concern and requires rapid and efficient neutralization methods. Herein, we report novel two-in-one light-driven micromotors, *i.e.*, light-driven TiO_2-Fe Janus micromotors with both photocatalysis and photo-Fenton processes, for efficiently degrading organic pollutants in contaminated water. The TiO_2-Fe micromotors moved rapidly by utilizing the photocatalytic H_2O_2 decomposition over TiO_2 under UV irradiation, as well as generating highly reactive oxygen species responsible for the *in situ* degradation of the organic pollutants into non-harmful products. Notably, such coupling of photocatalysis generated on the TiO_2 sides and the photo-Fenton process generated on the Fe sides, along with the rapid movement of these catalytic Janus micromotors, results in a synergetic effect that can greatly enhance the degradation of organic pollutants. The degradation efficiency of the TiO_2-Fe micromotors is 52-fold that of only Fenton effects, and it is further improved by 40% compared to photocatalytic degradation alone. Considering the excellent advantages of the high efficiency, simple structure, reusability and the bubble-driven property, the new "on-the-fly" TiO_2-Fe micromotor-based method has a promising potential for future water cleaning and waste-water treatments.

Introduction

Water pollution caused by organic pollutants has a harmful effect on the health of human beings and the living environment. Conventional cleaning methods such as physical adsorption, chlorination, and chemical precipitation are often unable to efficiently process these organic pollutants that are commonly found in industrial wastewater.[1] Therefore, the development of efficient methods for water treatment has always been a world-wide research focus.

Recent advancements in nanomaterials have provided more choices for the development of efficient water purification technologies.[2–6] Synthetic self-propelled micro/nanomotors, capable of converting energy into movement and forces, hold considerable potentials in various practical applications ranging from biological applications to environmental remediations.[7–17] Several types of micro/nanomotors have been developed, such as bimetallic catalytic nanowires, microtubular microrockets,[18] Janus microspheres,[19] and supramolecule-based nanomotors.[20] These micro/nanomotors can be efficiently propelled by light,[21] ultrasound,[22] magnetic field,[23] electrical field,[24] and chemical reactions.[12,25] In the field of water and environment remediation, especially compared with static counterparts, emerging micro/nanomotors not only inherit the excellent properties of micro/nanomaterials, such as high surface area and activity, but also demonstrate autonomous motion capacity, which both result in high efficiency for adsorption, chemical reactions, and catalysis. For instance, micro/nanomotors can efficiently collect residual oil droplets from water,[26] absorb heavy metal ions,[27] and degrade organic pollutants[28] by a proper structure design and surface functionalization. Owing to unique autonomous motion behavior and self-mixing without the external stirring of artificial micro/nanomotors, the micromotor-based methods can greatly enhance the contacts between pollutants and micro/nanomotors, and further lead to higher decontamination efficiencies and shorter clean-up times.[29] However, to the best of our knowledge, all of the micro/nanomotors applied in pollutant degradation are based on a single mechanism: either the photocatalysis or Fenton process. For example, Li *et al.*

[a]*School of Chemistry and Environment, South China Normal University, Guangzhou 510006, China. E-mail: rfdong@m.scnu.edu.cn, caiyp@scnu.edu.cn*
[b]*Department of Materials Science, Fudan University, Shanghai, 200433, China. E-mail: yongfeng.mei@gmail.com*

†Electronic supplementary information (ESI) available. See DOI: 10.1039/c9nr04295d

‡These authors contributed equally.

presented magnesium-based spherical micromotors coated with a photoactive titanium dioxide film for the photocatalytic decomposition of biological and chemical warfare agents.[29] Parmar *et al.* developed cobalt-ferrite-based micromotors for the efficient degradation of tetracycline antibiotics from water.[30] While photocatalysis needs light illumination, the Fenton process requires an acidic environment. These strict requirements for each effect have greatly limited the application range of such motors, whereas the efficiency of pollutant degradation has been limited by the single mechanism. In order to expand the applications of synthetic micro/nanomotors, overcoming the challenges of developing artificial micro/nanomotors that not only have multiple degradation mechanisms to tackle the complicated water environment in real world, but also exhibit high efficiency for pollutant degradation, has become critically important.

In the present study, we report a novel two-in-one light-driven micromotors, that is, highly efficient light-driven TiO_2-Fe Janus micromotors with both photocatalysis and photo-Fenton process for efficiently degrading organic pollutants in contaminated water. As shown in Scheme 1, the Janus micromotors consist of plain TiO_2 particles (~15.0 μm mean diameter) with one hemisphere coated with Fe metal. In the presence of H_2O_2, the TiO_2-Fe micromotors moved rapidly by utilizing the photocatalytic H_2O_2 decomposition over TiO_2 under UV irradiation. Moreover, the photocatalysis generated on the TiO_2 sides and the photo-Fenton process generated on the Fe sides integrated into one micromotor, resulting in a strong synergetic effect which could greatly enhance the degradation of the organic pollutants. Rhodamine 6G (Rh6G) was chosen as a model pollutant to demonstrate the water remediation efficiency. The combination of the photocatalysis and photo-Fenton processes resulted in the removal rate of Rh6G being *ca.* 52 times faster than that when the degradation process was carried out with only the Fenton process; also, the degradation rate was 40% higher compared to photocatalytic degradation alone. In addition, unlike most photocatalytic micro/nanomotors applied in environmental remediation, such TiO_2-Fe micromotors can be reused merely by magnetic separation due to the magnetic properties of Fe, thus exhibiting excellent reusability. Owing to the advantages of its simple structure and outstanding reusability, the novel "on-the-fly" TiO_2-Fe micromotors manifest great prospects in improving the efficiency of water cleaning and pave the way for using the new micromotors for environmental applications.

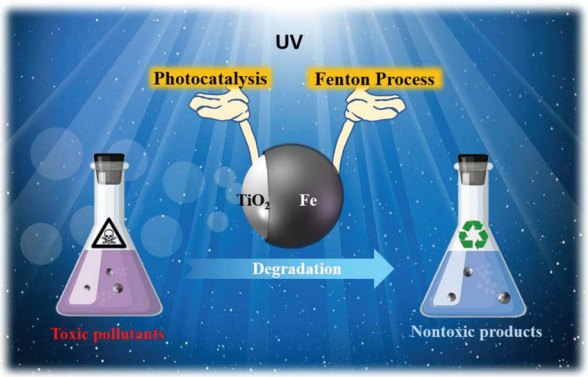

Scheme 1 Schematic process for the degradation of polluted water into inorganic products by TiO_2-Fe self-propelled micromotors by the combination of photocatalytic degradation and photo-Fenton process. The self-propulsion is achieved by the catalytic activity of TiO_2 under UV irradiation, which provides the motion of the micromotors in H_2O_2 solutions.

Experiments section

Chemicals and reagents

Tetrabutyl titanate (TBT) was purchased from Sigma-Aldrich. Octanoic acid (CA) and polyvinyl alcohol were purchased from Aladdin Chemistry Co., Ltd. All other chemical reagents were purchased from Shanghai Chemical Reagent Company.

Synthesis of TiO_2 microspheres

TiO_2 microspheres were prepared by the O/W microemulsion method according to a previous report.[31] First, the oil phase of 2 mL CA solution with 10 wt% TBT was added into the aqueous solution of 40 mL polyvinyl alcohol (2 wt%). Then, the mixture was magnetically stirred for 2 min to form TBT/CA microdroplets in the aqueous solution. Following this, 4.5 mL ammonia (25 wt%) was used to trigger the hydrolysis of TBT/CA droplets, and the solution was stirred for another 5 min. After standing for 24 h, TiO_2 microspheres (15 μm mean diameter) were obtained. The obtained TiO_2 microspheres were washed 8 times with deionized water and 3 times with ethanol. In order to obtain the TiO_2 (anatase) microsphere, the obtained TiO_2 microspheres were dried in air at 50 °C, and then annealed for 2 h at 400 °C.

Preparation of TiO_2-Fe Janus microspheres

For preparing the TiO_2-Fe light-driven Janus micromotor, TiO_2 microspheres (15 μm mean diameter) were used as the base particles. Initially, 200 μL of TiO_2 microspheres dispersed in ethanol was dropped on a glass slide and dried at 80 °C for 5 min. Then, the sample was spread onto glass slides and dried uniformly to form particle monolayers. Subsequently, the exposed surfaces of the TiO_2 microspheres were coated with a Fe layer *via* an ion sputtering instrument (Beijing Ruifu Si Technology Co., Ltd VTC300) for 5 min under the condition of 40 sccm of Ar flow rate, 2.2 Pa air pressure, and 90 W RF power. The TiO_2-Fe Janus microspheres were then separated from the glass slide by an ultrasonication process. The size and morphology of the TiO_2-Fe micromotor were characterized by scanning electron microscopy (SEM, Tescan MAIA 3) and optical microscopy. The thickness of the Fe coating on TiO_2 was measured by the Form Talysruf Profiler. The crystal structure of TiO_2-Fe was characterized by X-ray diffraction (XRD, Bruker D8 Advance). Element distribution in TiO_2-Fe was investigated on an Oxford x-act analyser.

TiO_2-Fe Janus micromotor propulsion

The autonomous propulsion of the TiO_2-Fe micromotors was obtained in a solution containing 5% H_2O_2 and 1 wt% sodium dodecyl sulfate (SDS) as a surfactant. Videos were captured by an inverted optical microscope (Nikon Instrument Inc. Ti-S/L100) using the NIS Elements AR 3.2 software.

Photocatalytic experiments

Rh6G degradation experiments were performed by adding TiO_2-Fe micromotors into a solution of 600 μL at an initial pH = 2.5 (adjusting the pH with HCl), with Rh6G (C_0 = 5 mg L^{-1}), 5% H_2O_2, 1 wt% SDS, and TiO_2-Fe micromotors (10 mg mL^{-1}). A hand-held UV lamp with a power density of 1.8 mW cm^{-2} was used to irradiate the sample (Shanghai Jiapeng Technology Co., Ltd, model: ZF5, radiation wavelength: 365 nm). After the photochemical reaction, the absorbance of the solution was measured using a UV-vis spectrophotometer (UV-2450, Shimadzu). The value of the UV absorbance at 563 nm (A_{563}) was used to quantitatively evaluate the degree of degradation. For the reusability experiment, after recording the UV absorbance of each round, the TiO_2-Fe micromotors were separated by a magnet, and then added into the new solution, as described in the previous Rh6G degradation experiments. Controlled experiments of static TiO_2-Fe micromotors were performed in the absence of H_2O_2 or UV. The degradation experiments were carried out under standard conditions (298 K and 1 atm).

Results and discussion

Characterization of the structure of the Janus TiO_2-Fe micromotors

To achieve efficient degradation of organic pollutants in water with both photocatalysis and the photo-Fenton process, we fabricated the new two-in-one light-driven TiO_2-Fe Janus micromotors by coating an Fe layer on one hemisphere surface of TiO_2 microspheres. Scanning electron microscopy (SEM) was carried out to examine the size and morphology of the TiO_2-Fe micromotors. As shown in the inset of Fig. 1, the inset SEM image displays the morphology of these prepared TiO_2-Fe micromotors, with a relatively uniform spherical shape and approximately an average size of 15 μm. Moreover, the crystal structure of TiO_2-Fe was characterized by XRD, as shown in Fig. 1A, where it was noted that all diffraction peaks were characteristic of the orthogonal TiO_2-Fe. The SEM image of Fig. 1B displays the morphology of a prepared TiO_2-Fe micromotor, in which the surface of the TiO_2 microsphere with one hemisphere is coated with an Fe layer. The corresponding energy-dispersive X-ray spectroscopy (EDX) mapping of Ti, Fe, and O displayed in Fig. 1C, D, E, respectively, has further confirmed the Janus structure of such a micromotor.

Photocatalytic propulsion of the TiO_2-Fe Janus micromotors

The TiO_2-Fe Janus micromotor exhibited attractive photocatalytic propulsion, which was crucial for efficient degradation of the pollutants. As illustrated in Fig. 2A, upon UV irradiation of the Janus micromotors, charge separation occurred within TiO_2 and electrons were injected from the TiO_2 conduction band into the Fe hemisphere. O_2 gas was produced from the oxidation of H_2O_2 at TiO_2 and the resulting electrons were consumed during the reduction of protons at Fe. As a result, without UV light, the motors were motionless (Fig. 2B); however, once UV light (wavelength λ = 368 nm) was turned on, a long tail of O_2 bubbles was generated on one side of the TiO_2, propelling the micromotor in the opposite direction (Fig. 2C). The average speed of such a TiO_2-Fe Janus micromotor could reach up to ~260 μm s^{-1} with 5 wt% H_2O_2 and 1 wt% sodium dodecyl sulfate (SDS) and under UV light. To the best of our knowledge, this is the fastest spherical bubble-driven micromotor obtained so far under the same fuel concentration and with similar size.[29,31]

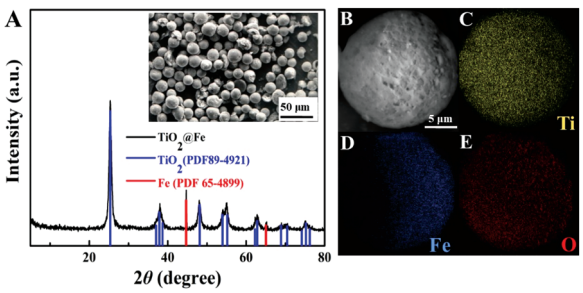

Fig. 1 (A) The XRD pattern of TiO_2-Fe micromotors. The inset shows the SEM image of TiO_2-Fe micromotors with an average diameter around 15 μm. Scale bar, 50 μm. (B) SEM image of a spherical TiO_2-Fe Janus micromotor. (C–E) The corresponding EDX mapping images for Ti, Fe, and O, respectively.

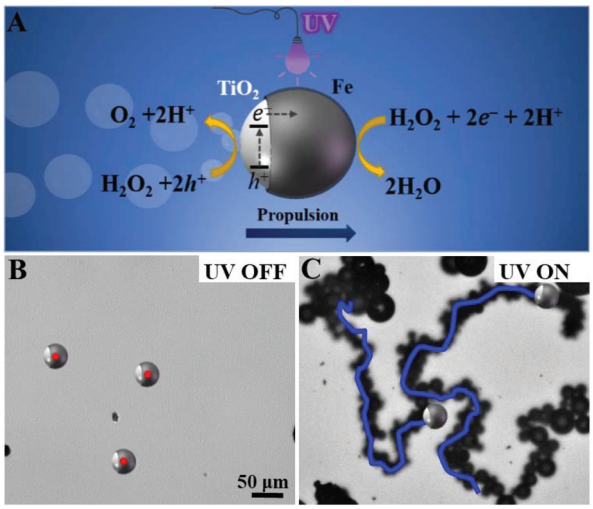

Fig. 2 Motion behavior of the TiO_2-Fe Janus micromotor. (A) Schematic of the propulsion mechanism of the TiO_2-Fe micromotors. (B) The image illustrating the state of the micromotor without UV light. (C) Tracking line image illustrating the micromotors' propulsion over a 1 s period in 5 wt% H_2O_2 with 1 wt% sodium dodecyl sulfate (SDS) (all the images were taken from ESI Video S1†).

Degradation of dyes by micromotors

The TiO_2-Fe Janus micromotors exhibited excellent degradation activity by coupling the two popular degradation mechanisms. On their UV-activated TiO_2 surfaces, these TiO_2-Fe micromotors generated highly oxidative species and moved autonomously by utilizing the photocatalytic H_2O_2 decomposition, resulting in a significant photocatalytic decontamination process. On their Fe surfaces, ions were generated by oxidizing the metallic Fe on the surface of the micromotors in acidic media in a thermodynamically spontaneous process, enabling a remarkably effective photo-Fenton cleaning system between *in situ* generated Fe ions and hydrogen peroxide (Fig. 3A).[1,29] It is clear from Fig. 3B that the UV-vis absorbance spectrum of Rh6G drastically decreased with the increase in remediation time following 12 min treatment with the active TiO_2-Fe Janus micromotors under UV light irradiation. The results indicate that the active micromotors exhibit highly efficient degradation of Rh6G.

Systematic control experiments were performed to confirm the improvement in degradation efficiency by the employment of the two-in-one self-propelled TiO_2-Fe micromotors with both photocatalysis and photo-Fenton process. The value of the UV absorbance at 563 nm (A_{563}) was used to quantitatively evaluate the degree of Rh6G degradation. In this system, UV light is essential for photocatalysis while pH value and Fe is significant for the photo-Fenton process, and UV and H_2O_2 are the basic requirements for bubble propulsion. As shown in Fig. 3C, the highest Rh6G degradation efficiency corresponding to ~95% can be achieved at about 12 min with all the necessary conditions, including TiO_2-Fe micromotors, UV irradiation, H_2O_2 and proper pH. This indicated that both the photocatalysis and photo-Fenton processes were generated within the active photocatalytic micromotors (Fig. 3C-a). However, without HCl (Fig. 3C-b), no Fenton reactions took place and only photocatalytic effects were generated by the active motors, causing the degradation efficiency to decrease to 70%. At the same condition of the H_2O_2, HCl and UV light, the degradation efficiency of the same amount of TiO_2 and Fe was ~41% (Fig. 3C-c), which is

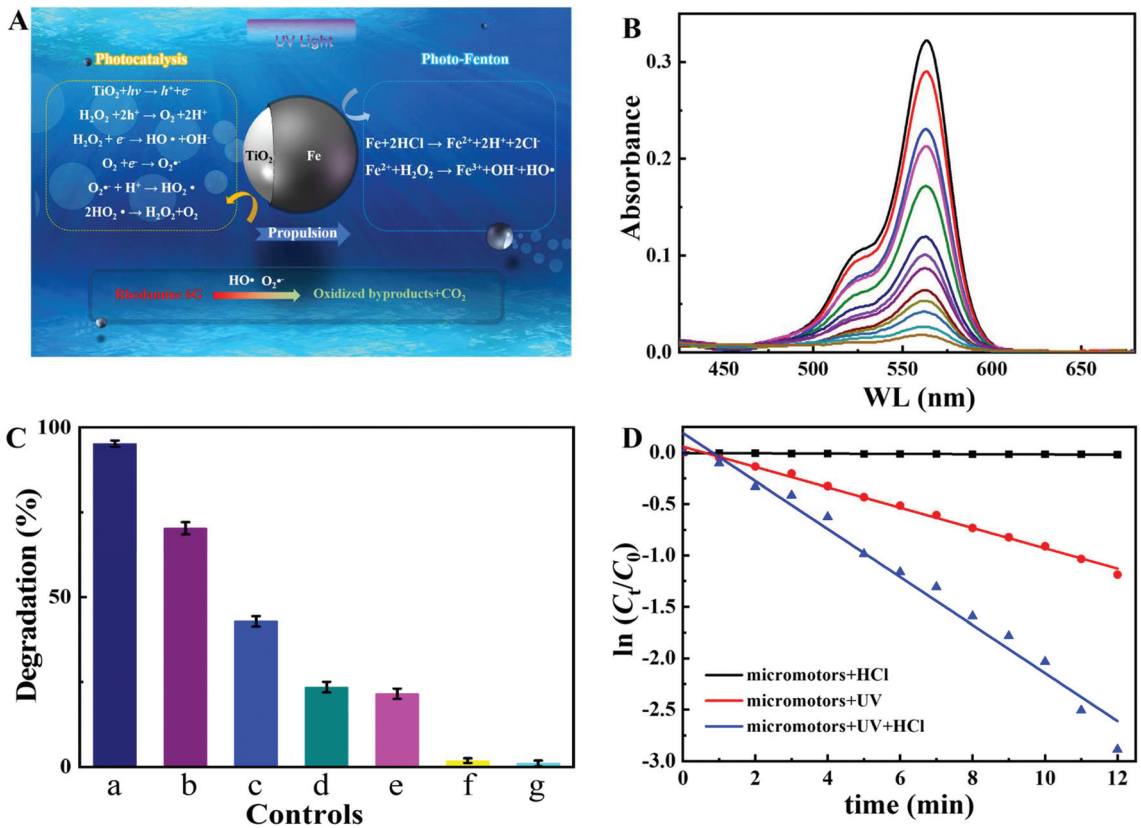

Fig. 3 The "on-the-fly" degradation of Rh6G using TiO_2-Fe micromotors. (A) The principle of the degradation of polluted water (rhodamine 6G as model contaminant) into inorganic products by TiO_2-Fe micromotors by the combination of photocatalytic degradation and Fenton process. (B) The absorbance spectra of Rh6G over time with micromotors with UV irradiation at pH 2.5, with Rh6G (C_0 = 5 mg L^{-1}), 5% H_2O_2, 1% SDS as surfactant in a total volume of 600 μL. (C) The histogram of the photodegradation efficiency of Rh6G after a 10 min treatment with micromotors under different conditions (a: Rh6G + TiO_2-Fe micromotors + H_2O_2 + UV + HCl; b: Rh6G + TiO_2-Fe micromotors + H_2O_2 + UV without HCl; c: Rh6G + TiO_2 + Fe + H_2O_2 + UV + HCl; d: Rh6G + TiO_2-Fe micromotors + UV + HCl without H_2O_2; e: Rh6G + TiO_2 + H_2O_2 + UV + HCl; f: Rh6G + TiO_2-Fe micromotors + H_2O_2 + HCl without UV; g: blank control (Rh6G + H_2O_2 + UV + HCl)). (D) The photodegradation of Rh6G over time with micromotors and H_2O_2 under different conditions (black line: Rh6G + TiO_2-Fe micromotors + HCl without UV; red line: Rh6G + TiO_2-Fe micromotors + UV without HCl; blue line: Rh6G + TiO_2-Fe micromotors + UV + HCl).

much lower than that of the moved TiO_2-Fe micromotors. In Addition, if the system was without H_2O_2 (Fig. 3C-d), no O_2 bubbles were generated; thus, although photocatalysis was observed, the motors remained static; therefore, the degradation efficiency decreased due to the absence of self-mixing. It should be noted that the degradation efficiency of active TiO_2-Fe micromotors was 5-fold higher than that of active plain TiO_2 microspheres (Fig. 3C-e), which was attributed to metal introduction that could efficiently enhance the charge separation of TiO_2 under UV light. Finally, without UV light (Fig. 3C-f), neither bubble propulsion was generated nor photocatalysis took place. Only very slight degradations were observed (1.8%) over 12 min due to the low degradation efficiency of the Fenton effect only without active motors. The pollutant degradation efficiency of the active TiO_2-Fe micromotors was 52 times higher than that of static TiO_2-Fe microparticles with only Fenton effects. It was therefore clearly indicated that the active two-in-one TiO_2-Fe Janus micromotors improved the efficiency of the oxidation of Rh6G.

In addition, the comparison of the results of Rh6G degradation rate under different conditions further confirms the advantages of such two-in-one TiO_2-Fe Janus micromotors. As plotted in Fig. 3D, the photodegradation of Rh6G followed the first-order kinetics model, where C_0 and C_t are the initial concentration and the concentration at time t, respectively, and k is the first-order rate constant.

$$\ln\frac{C_t}{C_0} = kt$$

As shown, the highest k value (23.34×10^{-2}) was obtained using TiO_2-Fe micromotors under UV irradiation in the solution containing H_2O_2 and HCl, which indicates that both the photocatalysis and photo-Fenton process were generated within the active photocatalytic micromotors (Fig. 3D, blue line). However, without UV radiation (Fig. 3D, black line, static motors with Fenton effects only) or HCl (Fig. 3D, red line, active motors with photocatalysis only), the k values decreased to 0.13×10^{-2} and 9.88×10^{-2}, respectively. All the above results clearly illustrate that a synergetic effect for organic pollutant degradation was effectively achieved by taking advantage of the novel self-propelled micromotors with both the photocatalysis and photo-Fenton processes, indicating considerable promise for water cleaning.

Reusability of the TiO_2-Fe micromotors for the dyes degradation

Of particular significance, these TiO_2-Fe micromotors showed excellent reusability by magnetic separation because the novel TiO_2-Fe micromotors possessed remarkable magnetic pro-

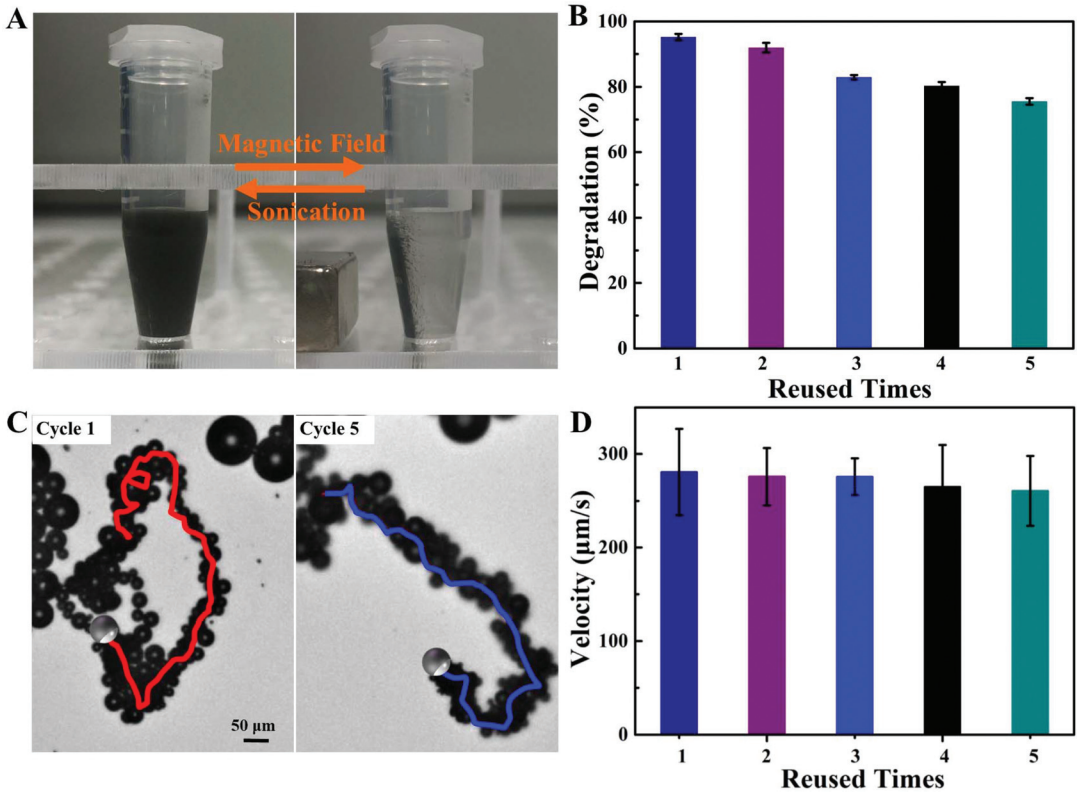

Fig. 4 Reusability of the TiO_2-Fe micromotors. (A) The photo of the micromotors without or with external magnetic field. (B) The histogram of the photodegradation efficiency of Rh6G after a 10 min treatment with the same micromotors for 5 times. (C) The time-lapse images show the propulsion of micromotors over a 1 s period for using for the first and fifth cycling treatment with Rh6G, respectively (all the taken from ESI Video S2†). (D) The histogram of the speed of the micromotor *vs.* the recycles times. All samples were prepared at pH 2.5, with Rh6G (C_0 = 5 mg L^{-1}), 5% H_2O_2, 1% SDS as surfactant in a total volume of 600 μL.

perties. The magnetic iron layer of the TiO_2-Fe micromotors not only played a key role in the photo-Fenton process, which could enhance the degradation efficiency, but also allowed the micromotors to be separated under an external magnetic field (Fig. 4A). Fig. 4B clearly illustrates the photodegradation efficiency of Rh6G after a 12 min treatment with the same micromotors for 5 times. As expected, even after recycling for the fifth time, the degradation efficiency can be reach 75%. The decrease in degradation could be related to iron losses due to the iron being dissolved at acidic pH used for the experiment. The concentration of the released Fe ions in the aqueous solution after the degradation was analyzed by inductively coupled plasma optical emission spectrometry (ICP-OES). After 1 cycle of the experiment, the content of Fe was determined to be about 0.91 mg L^{-1}. In order to further confirm the reason for such reusability, the population of the TiO_2-Fe micromotors after using for 5 times was investigated. As shown in Fig. 4C, the tracking line image showed that there was no significant change in the propulsion of the micromotors between cycle 1 and cycle 5 (the images were taken from the corresponding Video S2 in ESI†). In addition the average speed of the micromotors *vs.* each cycle was calculated. The results (Fig. 4D) illustrated that the recycle times had a negligible impact on the speed of the micromotors and the TiO_2-Fe Janus micromotors also exhibited excellent photocatalytic propulsion. These results reasonably explained why the micromotors could still maintain efficient degradation after reusing and provide a prerequisite for the reuse of the TiO_2-Fe micromotors for efficient water remediation. Such novel TiO_2-Fe micromotors with excellent reusability would facilitate the application of micro/nanomotors in environmental remediation.

Conclusions

In conclusion, for the first time, we have reported novel two-in-one light-driven TiO_2-Fe Janus micromotors that integrate two popular degradation mechanisms (photocatalysis and photo-Fenton process) in one motor for highly efficient organic pollutant degradation in a water environment. The "on-the-fly" degradation process based on the active TiO_2-Fe Janus micromotors resulted in a highly efficient removal of Rhb6, which was *ca.* 52 times faster than that when the degradation was carried out with only Fenton process. Compared with photocatalytic degradation alone, the degradation efficiency was increased by 40%. The enhanced photocatalytic degradation activity was attributed to the synergetic effect of the photocatalysis generated on the TiO_2 sides and photo-Fenton processes generated on the Fe sides. Advantageously, the TiO_2-Fe micromotors could be easily reused merely by magnetic separation. In view of the advantages of the high efficiency, simple structure and reusability, as well as the bubble-driven property, the novel "on-the-fly" TiO_2-Fe micromotors are expected to provide a powerful strategy for water purification and have great significance in practical water cleaning.

Conflicts of interest

There are no conflicts to declare.

Acknowledgements

The project received financial support from the National Natural Science Foundation of China (21805096, 21671071, 21471061), Natural Science Foundation of Guangdong Province (2018A030313358, 2017A030310432), Applied Science and Technology Planning Project of Guangdong Province, Guangzhou, China (2015B010135009, 2017B090917002), Innovation Team Project of Guangdong Ordinary University (2015KCXTD005), and the Great Scientific Research Project of Guangdong Ordinary University (2016KZDXM023).

Notes and references

1 L. Soler, V. Magdanz, V. M. Fomin, S. Sanchez and O. G. Schmidt, *ACS Nano*, 2013, **7**, 9611–9620.
2 P. G. Tratnyek and R. L. Johnson, *Nano Today*, 2006, **1**, 44–48.
3 M. S. Mauter and M. Elimelech, *Environ. Sci. Technol.*, 2008, **42**, 5843–5859.
4 M. M. Khin, A. S. Nair, V. J. Babu, R. Murugan and S. Ramakrishna, *Energy Environ. Sci*, 2012, **5**, 8075–8109.
5 W. Liu, F. Huang, Y. Wang, T. Zou, J. Zheng and Z. Lin, *Environ. Sci. Technol.*, 2011, **45**, 1955–1961.
6 W. Liu, F. Huang, Y. Liao, J. Zhang, G. Ren, Z. Zhuang, J. Zhen, Z. Lin and C. Wang, *Angew. Chem., Int. Ed.*, 2008, **47**, 5619–5622.
7 M. Safdar, S. U. Khan and J. Jänis, *Adv. Mater.*, 2018, **30**, 1703660.
8 J. Wang, *Nanomachines: Fundamentals and Applications*, Wiley-VCH, Weinheim, Germany, 2013.
9 T. E. Mallouk and A. Sen, *Powering nanorobots*, 2009.
10 J. J. Abbott, K. E. Peyer, L. X. Dong and B. J. Nelson, *Robot. Res.*, 2010, **66**, 157–167.
11 W. Gao and J. Wang, *ACS Nano*, 2014, **8**, 3170–3180.
12 M. Safdar, S. U. Khan and J. Jänis, *Adv. Mater.*, 2018, **30**, 1703660.
13 J. Li, B. Esteban-Fernández de Ávila, W. Gao, L. Zhang and J. Wang, *Sci. Robot.*, 2017, **2**, eaam6431.
14 K. Kim, J. Guo, Z. Liang and D. Fan, *Adv. Funct. Mater.*, 2018, **28**, 1705867.
15 S. Pané, J. Puigmartí-Luis, C. Bergeles, X. Z. Chen, E. Pellicer, J. Sort, V. Počepcová, A. Ferreira and B. J. Nelson, *Adv. Mater. Technol.*, 2018, **4**, 1800575.
16 F. Mou, L. Kong, C. Chen, Z. Chen, L. Xu and J. Guan, *Nanoscale*, 2016, **8**, 4976–4983.
17 F. Mou, D. Pan, C. Chen, Y. Gao, L. Xu and J. Guan, *Adv. Funct. Mater.*, 2015, **25**, 6173–6181.
18 B. Xu, B. Zhang, L. Wang, G. Huang and Y. Mei, *Adv. Funct. Mater.*, 2018, **28**, 1705872.

19 Z. Wu, L. Li, T. Liao, X. Chen, W. Jiang, W. Luo, J. Yang and Z. Sun, *Nano Today*, 2018, **22**, 62–82.
20 I. Ortiz-Rivera, M. Mathesh and D. A. Wilson, *Acc. Chem. Res.*, 2018, **51**, 1891–1900.
21 J. Wang, Z. Xiong, J. Zheng, X. Zhan and J. Tang, *Acc. Chem. Res.*, 2018, **51**, 1957–1965.
22 T. Xu, L.-P. Xu and X. Zhang, *Appl. Mater. Today*, 2017, **9**, 493–503.
23 P. Mandal, G. Patil, H. Kakoty and A. Ghosh, *Acc. Chem. Res.*, 2018, **51**, 2689–2698.
24 L. Bouffier, V. Ravaine, N. Sojic and A. Kuhn, *Curr. Opin. Colloid Interface Sci.*, 2016, **21**, 57–64.
25 X. Zhao, K. Gentile, F. Mohajerani and A. Sen, *Acc. Chem. Res.*, 2018, **51**, 2373–2381.
26 M. Guix, J. Orozco, M. García, W. Gao, S. Sattayasamitsathit, A. Merkoçi, A. Escarpa and J. Wang, *ACS Nano*, 2012, **6**, 4445–4451.
27 D. Vilela, J. Parmar, Y. Zeng, Y. Zhao and S. Sánchez, *Nano Lett.*, 2016, **16**, 2860–2866.
28 L. Kong, C. C. Mayorga-Martinez, J. Guan and M. Pumera, *ACS Appl. Mater. Interfaces*, 2018, **10**, 22427–22434.
29 J. Li, V. V. Singh, S. Sattayasamitsathit, J. Orozco, K. Kaufmann, R. Dong, W. Gao, B. Jurado-Sanchez, Y. Fedorak and J. Wang, *ACS Nano*, 2014, **8**, 11118–11125.
30 J. Parmar, K. Villa, D. Vilela and S. Sánchez, *Appl. Mater. Today*, 2017, **9**, 605–611.
31 Y. Li, F. Mou, C. Chen, M. You, Y. Yin, L. Xu and J. Guan, *RSC Adv.*, 2016, **6**, 10697–10703.